

Accurate and efficient splitting methods for dissipative particle dynamics

Xiaocheng Shang*

School of Mathematics, University of Birmingham, Edgbaston, Birmingham, B15 2TT, United Kingdom

May 12, 2020

Abstract

We study numerical methods for dissipative particle dynamics (DPD), which is a system of stochastic differential equations and a popular stochastic momentum-conserving thermostat for simulating complex hydrodynamic behavior at mesoscales. We show that novel splitting methods are able to substantially improve the accuracy and efficiency of DPD simulations in a wide range of the friction coefficients, particularly in the extremely large friction limit that corresponds to a fluid-like Schmidt number, a key issue in DPD. Various numerical experiments are performed to demonstrate the superiority of the newly proposed methods over popular alternative schemes in the literature.

1 Introduction

Since its introduction by Hoogerbrugge and Koelman [21] at the end of the last century and due to its algorithmic simplicity and modelling versatility, DPD has become a popular stochastic momentum-conserving thermostat for simulating complex hydrodynamic behavior at a mesoscopic level [19, 53]. Unlike individual molecules, DPD particles represent groups of fluid molecules and interact at short range with a soft potential. The coarse-grained descriptions allow the use of time and length scales that would otherwise be inaccessible by conventional molecular dynamics at microscales [5, 17]. Therefore, DPD has been widely used in a large number of complex fluids and soft matter applications, including colloids [24], blood [16], and polymers [54] (see more applications in an excellent recent review [14] and references therein).

1.1 Formulation of DPD

Originally updated in discrete time steps, DPD was later reformulated by Español and Warren [13] as a proper statistical mechanics model that is a system of Itô stochastic differential equations (SDEs). Consider an N -particle system evolving in dimension d with position $\mathbf{q}_i \in \mathbb{R}^d$, momentum $\mathbf{p}_i \in \mathbb{R}^d$, and mass $m_i \in \mathbb{R}$ for $i = 1, \dots, N$, the equations of motion for

*Corresponding author. Email: x.shang.1@bham.ac.uk

DPD particles are given by

$$d\mathbf{q}_i = m_i^{-1} \mathbf{p}_i dt, \quad (1a)$$

$$d\mathbf{p}_i = \sum_{j \neq i} \mathbf{F}_{ij}^C(r_{ij}) dt - \gamma \sum_{j \neq i} \omega^D(r_{ij}) (\mathbf{e}_{ij} \cdot \mathbf{v}_{ij}) \mathbf{e}_{ij} dt + \sigma \sum_{j \neq i} \omega^R(r_{ij}) \mathbf{e}_{ij} dW_{ij}, \quad (1b)$$

where \mathbf{F}_{ij}^C is the conservative force acting along the line of centres, typically chosen as [19]

$$\mathbf{F}_{ij}^C(r_{ij}) = \begin{cases} a_{ij}(1 - r_{ij}/r_c) \mathbf{e}_{ij}, & r_{ij} < r_c; \\ 0, & r_{ij} \geq r_c, \end{cases} \quad (2)$$

where parameter a_{ij} represents the maximum repulsion strength between particles i and j , $r_{ij} = |\mathbf{q}_{ij}| = |\mathbf{q}_i - \mathbf{q}_j|$ is the distance, and r_c denotes a certain cutoff radius. Moreover, $\mathbf{e}_{ij} = \mathbf{q}_{ij}/r_{ij}$ represents the unit vector pointing from particle j to particle i , $\mathbf{v}_{ij} = \mathbf{p}_i/m_i - \mathbf{p}_j/m_j$ denotes the relative velocity, and $dW_{ij} = dW_{ji}$ are independent increments of the Wiener process with mean zero and variance dt . Parameters γ and σ , representing the dissipative and random strengths, respectively, and position-dependent weight functions ω^D and ω^R are required to satisfy the following fluctuation-dissipation relation for DPD:

$$\sigma^2 = 2\gamma k_B T, \quad \omega^D(r_{ij}) = [\omega^R(r_{ij})]^2, \quad (3)$$

where k_B is the Boltzmann constant and T is the equilibrium temperature. Note that one of the two weight functions can be arbitrarily chosen, for instance, a popular choice of ω^R is

$$\omega^R(r_{ij}) = \begin{cases} 1 - r_{ij}/r_c, & r_{ij} < r_c; \\ 0, & r_{ij} \geq r_c, \end{cases} \quad (4)$$

which fixes the other weight function ω^D . It can then be easily shown that the canonical ensemble is preserved with an invariant measure defined by the density

$$\rho_\beta(\mathbf{q}, \mathbf{p}) = Z^{-1} \exp(-\beta H(\mathbf{q}, \mathbf{p})), \quad (5)$$

where $\beta^{-1} = k_B T$, Z is a suitable normalizing constant (i.e., the partition function), and $H(\mathbf{q}, \mathbf{p})$ denotes the Hamiltonian defined as

$$H(\mathbf{q}, \mathbf{p}) = \sum_i \frac{\mathbf{p}_i \cdot \mathbf{p}_i}{2m_i} + U(\mathbf{q}), \quad (6)$$

where U is the potential energy

$$U(\mathbf{q}) = \sum_i \sum_{j > i} \varphi(r_{ij}), \quad (7)$$

with $\varphi(r_{ij})$ being the soft pair potential energy, corresponding to the conservative force (2)

$$\varphi(r_{ij}) = \begin{cases} a_{ij}r_c(1 - r_{ij}/r_c)^2/2, & r_{ij} < r_c; \\ 0, & r_{ij} \geq r_c. \end{cases} \quad (8)$$

Due to the pairwise (or symmetric) nature of the interactions between particles and also the dependence on relative velocities, both linear and angular momenta are conserved in DPD. Moreover, DPD is an isotropic Galilean-invariant thermostat that preserves hydrodynamics [4, 41, 53]. Note that if the linear momentum is conserved, the density (5) should be replaced by

$$\rho_\beta(\mathbf{q}, \mathbf{p}) = Z^{-1} \exp(-\beta H(\mathbf{q}, \mathbf{p})) \times \delta \left[\sum_i p_{i,x} - \pi_x \right] \delta \left[\sum_i p_{i,y} - \pi_y \right] \delta \left[\sum_i p_{i,z} - \pi_z \right], \quad (9)$$

where $\boldsymbol{\pi} = (\pi_x, \pi_y, \pi_z)$ is the linear momentum vector. A similar modification would also be needed for the angular momentum conservation. However, the angular momentum will not be conserved if either periodic boundary conditions or Lees–Edwards boundary conditions [27] (care should be taken when implemented in DPD, see more discussion in [36]) are applied. Note also that it is highly nontrivial to show the ergodicity of DPD, which has only been demonstrated in the case of high particle density in one dimension by Shardlow and Yan [52].

1.2 Schmidt number issue in DPD

The Schmidt number, Sc , is an important quantity that characterizes the dynamical behavior of fluids. It is the ratio of the kinematic viscosity ν (also called “momentum diffusivity”) to the diffusion coefficient D , and in a typical fluid flow (e.g., water), momentum is expected to be transported more rapidly than mass, leading to a Schmidt number of $O(10^3)$. However, it has been pointed out that the standard DPD formulation described in Section 1.1 (also known as the “model B” in the language of [42]), with a standard set of parameters (e.g., [3] with $\gamma = 4.5$), produces a gas-like Schmidt number of $O(1)$, resulting in concerns on the separation of the timescale for the propagation of hydrodynamic interactions and that for diffusion [19]. More precisely, the Schmidt number associated with the standard DPD formulation is approximated as

$$\text{Sc} = \frac{\nu}{D} \approx \frac{1}{2} + \frac{(2\pi\gamma\rho_d r_c^4)^2}{70875k_B T}, \quad (10)$$

where ρ_d is the particle density. Although we can easily see from the approximation above that the most efficient way to increase the Schmidt number is to extend the cutoff radius r_c , it is also obvious that it could result in a substantial computational overhead [15]. As discussed in [38], one could generate a larger viscosity by increasing the stiffness of the conservative force or the particle density. However, the represented length scale decreases in both approaches, thereby contradicting the intended coarse-graining property of the DPD method. Alternatively, it has been suggested by Groot and Warren in [19] that a larger value of the friction coefficient γ may be used, although the authors also mentioned that the largest stepsize usable may have to be reduced in order to maintain the temperature control. To this end, the aim of the current article is to explore if there exist numerical integrators that would allow the use of large stepsizes in potentially very high friction limit, producing a fluid-like Schmidt number, while maintaining good control of the temperature and other important physical quantities. To the best of our knowledge, we are not aware of such studies within the standard DPD formulation in the literature.

Although considerable effort has been devoted to developing accurate and efficient numerical methods where large stepsizes can be used while maintaining good equilibrium properties, the corresponding Schmidt numbers were often gas-like. Following early examinations on the

performance of various DPD integrators [6, 10, 42, 59], a number of popular methods (including the Lowe–Andersen (LA) thermostat [39], and its variant, the Nosé–Hoover–Lowe–Andersen (NHLA) thermostat [55]) have been systematically compared in two recent studies [34, 36]. In the current article, we demonstrate that the accuracy and efficiency of DPD simulations can be substantially improved in a wide range of the friction coefficients, especially in the extremely large friction limit (i.e., $\gamma = 450$) that corresponds to a fluid-like Schmidt number (i.e., $Sc \approx 1016$). It is worth mentioning that the Schmidt number can be varied by either modifying the weight function [15, 61] or using alternative approaches (e.g., LA and NHLA). However, in the current article we restrict our attention on the standard DPD formulation as it is by far the most popular and studied approach.

1.3 Outline of the article

The rest of the article is organized as follows. In Section 2, we first describe two popular integration methods for DPD, followed by the derivations of two new promising schemes. We also theoretically demonstrate the order of convergence for methods that successively integrate the dissipative and random forces based on interacting pairs. A variety of numerical experiments are performed in Section 3 to compare all the schemes described in the article with a wide range of the friction coefficients. Our findings are summarized in Section 4.

2 Numerical methods for DPD

In discussing the numerical integration of DPD, it is more convenient to rewrite the DPD system (1) to a more compact form:

$$d\mathbf{q}_i = m_i^{-1} \mathbf{p}_i dt, \quad (11a)$$

$$d\mathbf{p}_i = \mathbf{F}_i^C dt + \mathbf{F}_i^D dt + \mathbf{F}_i^R, \quad (11b)$$

where \mathbf{F}_i^C , \mathbf{F}_i^D , and \mathbf{F}_i^R respectively represent the total conservative, dissipative, and random forces acting on particle i ,

$$\mathbf{F}_i^C(\mathbf{q}) = \sum_{j \neq i} \mathbf{F}_{ij}^C(r_{ij}), \quad (12a)$$

$$\mathbf{F}_i^D(\mathbf{q}, \mathbf{p}) = -\gamma \sum_{j \neq i} \omega^D(r_{ij})(\mathbf{e}_{ij} \cdot \mathbf{v}_{ij})\mathbf{e}_{ij}, \quad (12b)$$

$$\mathbf{F}_i^R(\mathbf{q}) = \sigma \sum_{j \neq i} \omega^R(r_{ij})\mathbf{e}_{ij} dW_{ij}. \quad (12c)$$

2.1 The velocity Verlet method

Despite the significant advancement of numerical integrators for DPD in the past two decades (see a comprehensive review in [34]), the velocity Verlet (VV) method [6] remains one of the most popular DPD integrators in popular software packages (e.g., LAMMPS [43] and DL_MESO [45]) due to its ease of implementation (particularly in parallel computing). The

integration steps of the VV method read

$$\mathbf{p}_i^{n+1/2} = \mathbf{p}_i^n + [\Delta t \mathbf{F}_i^C(\mathbf{q}^n) + \Delta t \mathbf{F}_i^D(\mathbf{q}^n, \mathbf{p}^n) + \mathbf{F}_i^R(\mathbf{q}^n)] / 2, \quad (13a)$$

$$\mathbf{q}_i^{n+1} = \mathbf{q}_i^n + \Delta t m_i^{-1} \mathbf{p}_i^{n+1/2}, \quad (13b)$$

$$\mathbf{p}_i^{n+1} = \mathbf{p}_i^{n+1/2} + [\Delta t \mathbf{F}_i^C(\mathbf{q}^{n+1}) + \Delta t \mathbf{F}_i^D(\mathbf{q}^{n+1}, \mathbf{p}^{n+1/2}) + \mathbf{F}_i^R(\mathbf{q}^{n+1})] / 2. \quad (13c)$$

where Δt is the integration stepsize and dW_{ij} in the random force (12c) is replaced by $\sqrt{\Delta t} R_{ij}$ with R_{ij} being a normally distributed variable with zero mean and unit variance. Note that all the forces in (12) need to be computed only once in (13c) and are reused in the subsequent step, otherwise the factor associated with the random force (i.e., $\sqrt{\Delta t}/2$) would be different. The VV method is also known as MD-VV in [59] and DL_MESO, or the modified Verlet method in [51], and is equivalent to the GW integrator of Groot and Warren [19] when the variable factor is fixed as one half (i.e., $\lambda = 1/2$).

It is well known that the standard VV method in molecular dynamics is second order [20, 32]. However, due to the presence of the dissipative and random forces in DPD, only first order convergence to the invariant measure is expected [51]. It is worth mentioning a variant of the VV method, that is, the DPD-VV method [6], also included in DL_MESO. DPD-VV only differs from VV in performing an additional update of the dissipative forces at the end of the integration steps. Although it has been claimed in [42] that the additional update could improve the performance considerably (see also good overall performance of DPD-VV in [6, 59]), we have observed in [34] that the performance of DPD-VV is rather similar to that of the splitting method proposed by Shardlow [51]. Given that Shardlow's splitting method has been the most recommended DPD integrator in the literature [14, 37, 42], it was often used to represent the standard DPD formulation in comparison studies [36, 48]. Therefore, we will include it in our numerical experiments in Section 3, while excluding DPD-VV.

2.2 Shardlow's splitting method: DPD-S1

Splitting methods have been widely used in a range of systems, including Hamiltonian dynamics [20, 32], dissipative systems [49], and stochastic dynamics [35, 48]. It was Shardlow who first adopted and systematically examined the techniques in the DPD context. More specifically, the vector field of the DPD system (11) is decomposed into three parts, which we label as A, B, and O:

$$d \begin{bmatrix} \mathbf{q}_i \\ \mathbf{p}_i \end{bmatrix} = \underbrace{\begin{bmatrix} m_i^{-1} \mathbf{p}_i \\ \mathbf{0} \end{bmatrix}}_A dt + \underbrace{\begin{bmatrix} \mathbf{0} \\ \mathbf{F}_i^C \end{bmatrix}}_B dt + \underbrace{\begin{bmatrix} \mathbf{0} \\ \mathbf{F}_i^D dt + \mathbf{F}_i^R \end{bmatrix}}_O, \quad (14)$$

where the first two splitting pieces (A and B) represent the Hamiltonian (or deterministic) part of the system and the remaining O part, with positions fixed, is an Ornstein–Uhlenbeck (OU) process. In describing splitting methods, we use the formal notation of the generator of the diffusion as in [11, 46, 57]. The generators for each part of the system may be written out

as follows:

$$\mathcal{L}_A = \sum_i \frac{\mathbf{p}_i}{m_i} \cdot \nabla_{\mathbf{q}_i}, \quad (15a)$$

$$\mathcal{L}_B = \sum_i \mathbf{F}_i^C \cdot \nabla_{\mathbf{p}_i} = \sum_i \sum_{j>i} \mathcal{L}_{B_{ij}}, \quad \mathcal{L}_{B_{ij}} = \mathbf{F}_{ij}^C(r_{ij}) \cdot (\nabla_{\mathbf{p}_i} - \nabla_{\mathbf{p}_j}), \quad (15b)$$

$$\mathcal{L}_O = \sum_i \sum_{j>i} \mathcal{L}_{O_{i,j}}, \quad (15c)$$

where

$$\mathcal{L}_{O_{i,j}} = \left[-\gamma \omega^D(r_{ij}) (\mathbf{e}_{ij} \cdot \mathbf{v}_{ij}) + \frac{\sigma^2}{2} [\omega^R(r_{ij})]^2 \mathbf{e}_{ij} \cdot (\nabla_{\mathbf{p}_i} - \nabla_{\mathbf{p}_j}) \right] \mathbf{e}_{ij} \cdot (\nabla_{\mathbf{p}_i} - \nabla_{\mathbf{p}_j}). \quad (16)$$

The generator for the DPD system thus can be written as

$$\mathcal{L}_{DPD} = \mathcal{L}_A + \mathcal{L}_B + \mathcal{L}_O. \quad (17)$$

Moreover, the flow map (or phase space propagator) of the system may be given by the shorthand notation

$$\mathcal{F}_t = e^{t\mathcal{L}_{DPD}}, \quad (18)$$

where the exponential map is used to formally denote the solution operator. Furthermore, approximations of \mathcal{F}_t may be obtained as products (taken in different arrangements) of exponentials of the various splitting terms. For instance, the phase space propagation of Shardlow's S1 splitting method [51], termed DPD-S1, can be written as

$$\exp(\Delta t \hat{\mathcal{L}}_{DPD-S1}) = \exp(\Delta t \hat{\mathcal{L}}_O) \exp\left(\frac{\Delta t}{2} \mathcal{L}_B\right) \exp(\Delta t \mathcal{L}_A) \exp\left(\frac{\Delta t}{2} \mathcal{L}_B\right), \quad (19)$$

where $\exp(\Delta t \mathcal{L}_f)$ denotes the phase space propagator associated with the corresponding vector field f . Note that the steplengths associated with various operations are uniform and span the interval Δt . Therefore the B step in (19) is taken with a steplength of $\Delta t/2$, while a steplength of Δt is associated with the O step. It is worth pointing out that, in dealing with pairwise interactions in the OU process, it is desirable to further split the vector field O into each interacting pair. Therefore, the propagation of the O part in (19) should be more explicitly defined as

$$\exp(\Delta t \hat{\mathcal{L}}_O) = \exp(\Delta t \hat{\mathcal{L}}_{O_{N-1,N}}) \dots \exp(\Delta t \hat{\mathcal{L}}_{O_{1,3}}) \exp(\Delta t \hat{\mathcal{L}}_{O_{1,2}}). \quad (20)$$

Since the method of Brünger, Brooks, and Karplus (BBK) [9] used for successively integrating each interacting pair in the O part has been shown to give weak second order approximations [51], the propagation associated with each interacting pair may be given by

$$\exp(\Delta t \hat{\mathcal{L}}_{O_{i,j}}) = \exp(\Delta t [\mathcal{L}_{O_{i,j}} + O(\Delta t^2)]). \quad (21)$$

where $\mathcal{L}_{O_{i,j}}$ is defined in (16). Overall, the BBK method is successively used for each interacting pair in the OU process (part O), followed by the velocity Verlet method [40, 60] for the

Hamiltonian part where both A and B parts are solved exactly:

Step 1: for each interacting pair within cutoff radius ($r_{ij} < r_c$), in a successive manner [26],

$$\mathbf{p}_i^{n+1/4} = \mathbf{p}_i^n - K_{ij}(\mathbf{e}_{ij}^n \cdot \mathbf{v}_{ij}^n)\mathbf{e}_{ij}^n + \mathbf{J}_{ij}, \quad (22a)$$

$$\mathbf{p}_j^{n+1/4} = \mathbf{p}_j^n + K_{ij}(\mathbf{e}_{ij}^n \cdot \mathbf{v}_{ij}^n)\mathbf{e}_{ij}^n - \mathbf{J}_{ij}, \quad (22b)$$

$$\mathbf{p}_i^{n+2/4} = \mathbf{p}_i^{n+1/4} + \mathbf{J}_{ij} - \frac{K_{ij}}{1+2K_{ij}} \left[(\mathbf{e}_{ij}^n \cdot \mathbf{v}_{ij}^{n+1/4})\mathbf{e}_{ij}^n + 2\mathbf{J}_{ij} \right], \quad (22c)$$

$$\mathbf{p}_j^{n+2/4} = \mathbf{p}_j^{n+1/4} - \mathbf{J}_{ij} + \frac{K_{ij}}{1+2K_{ij}} \left[(\mathbf{e}_{ij}^n \cdot \mathbf{v}_{ij}^{n+1/4})\mathbf{e}_{ij}^n + 2\mathbf{J}_{ij} \right], \quad (22d)$$

where $K_{ij} = \gamma\omega^D(r_{ij}^n)\Delta t/2$ and $\mathbf{J}_{ij} = \sigma\omega^R(r_{ij}^n)\mathbf{e}_{ij}^n\sqrt{\Delta t}\mathbf{R}_{ij}^n/2$.

Step 2: for each particle i ,

$$\mathbf{p}_i^{n+3/4} = \mathbf{p}_i^{n+2/4} + (\Delta t/2)\mathbf{F}_i^C(\mathbf{q}^n), \quad (23a)$$

$$\mathbf{q}_i^{n+1} = \mathbf{q}_i^n + \Delta t m_i^{-1} \mathbf{p}_i^{n+3/4}, \quad (23b)$$

$$\mathbf{p}_i^{n+1} = \mathbf{p}_i^{n+3/4} + (\Delta t/2)\mathbf{F}_i^C(\mathbf{q}^{n+1}). \quad (23c)$$

Note that the conservative force \mathbf{F}_i^C needs to be computed only once in (23c), where the Verlet neighbor lists [60] are also updated. The interacting pairs needed in the subsequent step can then be easily identified from the lists.

As a shorthand, we may term the DPD-S1 method (19) OBAB (similarly, the S2 method of Shardlow would be equivalent to OBABO in the same language). It has been shown in [10, 51] that the accuracy of both methods are very close to each other in a number of physical quantities. Given that the S1 method is more efficient than S2 [51], in what follows only the S1 method will be examined as in [26, 34, 37, 42, 48, 57].

2.3 The ASA method

Alternatively, the vector field of the DPD system (11) can be separated into two parts, which we label as A and S:

$$d \begin{bmatrix} \mathbf{q}_i \\ \mathbf{p}_i \end{bmatrix} = \underbrace{\begin{bmatrix} m_i^{-1} \mathbf{p}_i \\ \mathbf{0} \end{bmatrix}}_{\mathbf{A}} dt + \underbrace{\begin{bmatrix} \mathbf{0} \\ \mathbf{F}_i^C dt + \mathbf{F}_i^D dt + \mathbf{F}_i^R \end{bmatrix}}_{\mathbf{S}}. \quad (24)$$

The corresponding operator of part A is exactly the same as in the DPD-S1 method (thus can also be solved exactly), while the operator of part S is the sum of the operators of B and O defined in Section 2.2:

$$\mathcal{L}_S = \mathcal{L}_B + \mathcal{L}_O. \quad (25)$$

Similar to the DPD-S1 method, the vector field S is further split into each interacting pair. Moreover, each interacting pair in the S part is exactly solvable (in the sense of distributional fidelity). More precisely, for each interacting pair, i and j ($j > i$), subtracting $d\mathbf{v}_j$ from $d\mathbf{v}_i$ and multiplying the unit vector \mathbf{e}_{ij} on both sides yields

$$m_{ij} d\mathbf{v}_{ij} = F_{ij}^C(r_{ij})dt - \gamma\omega^D(r_{ij})v_{ij}dt + \sigma\omega^R(r_{ij})dW_{ij}, \quad (26)$$

where $m_{ij} = m_i m_j / (m_i + m_j)$ is the “reduced mass”, $v_{ij} = \mathbf{e}_{ij} \cdot \mathbf{v}_{ij}$, and $F_{ij}^C = \mathbf{e}_{ij} \cdot \mathbf{F}_{ij}^C(r_{ij})$ is the magnitude of the conservative force (2). The above equation is also an OU process with the exact (in the sense of distributions) solution [23]

$$v_{ij}(t) = \frac{F_{ij}^C}{\tau m_{ij}} + e^{-\tau t} \left[v_{ij}(0) - \frac{F_{ij}^C}{\tau m_{ij}} \right] + \frac{\sigma \omega^R}{m_{ij}} \sqrt{\frac{1 - e^{-2\tau t}}{2\tau}} \mathbf{R}_{ij}, \quad (27)$$

where $\tau = \gamma \omega^D / m_{ij}$ and $v_{ij}(0)$ is the initial relative velocity. Thus the velocity increment can be obtained as

$$\Delta v_{ij} = v_{ij}(t) - v_{ij}(0) = \left[v_{ij}(0) - \frac{F_{ij}^C}{\tau m_{ij}} \right] (e^{-\tau t} - 1) + \frac{\sigma \omega^R}{m_{ij}} \sqrt{\frac{1 - e^{-2\tau t}}{2\tau}} \mathbf{R}_{ij}, \quad (28)$$

and the corresponding momenta can be updated as follows:

$$\mathbf{p}_i \leftarrow \mathbf{p}_i + m_{ij} \Delta v_{ij} \mathbf{e}_{ij}, \quad (29a)$$

$$\mathbf{p}_j \leftarrow \mathbf{p}_j - m_{ij} \Delta v_{ij} \mathbf{e}_{ij}, \quad (29b)$$

which defines the propagator, $\exp(\Delta t \mathcal{L}_{S_{i,j}})$, for each interacting pair. Subsequently, we propose a new method, which we term the ASA method, whose propagator can be written as

$$\exp(\Delta t \hat{\mathcal{L}}_{ASA}) = \exp\left(\frac{\Delta t}{2} \mathcal{L}_A\right) \exp(\Delta t \hat{\mathcal{L}}_S) \exp\left(\frac{\Delta t}{2} \mathcal{L}_A\right), \quad (30)$$

where the propagation of the S part is defined as

$$\exp(\Delta t \hat{\mathcal{L}}_S) = \exp(\Delta t \mathcal{L}_{S_{N-1,N}}) \dots \exp(\Delta t \mathcal{L}_{S_{1,3}}) \exp(\Delta t \mathcal{L}_{S_{1,2}}). \quad (31)$$

The detailed integration steps of the ASA method read:

Step 1: for each particle i ,

$$\mathbf{q}_i^{n+1/2} = \mathbf{q}_i^n + (\Delta t/2) m_i^{-1} \mathbf{p}_i^n. \quad (32)$$

Step 2: for each interacting pair within cutoff radius ($r_{ij} < r_c$), in a successive manner,

$$\mathbf{p}_i^{n+1} = \mathbf{p}_i^n + m_{ij} \Delta v_{ij} \mathbf{e}_{ij}^{n+1/2}, \quad (33a)$$

$$\mathbf{p}_j^{n+1} = \mathbf{p}_j^n - m_{ij} \Delta v_{ij} \mathbf{e}_{ij}^{n+1/2}, \quad (33b)$$

with

$$\Delta v_{ij} = \left[\mathbf{e}_{ij}^{n+1/2} \cdot \mathbf{v}_{ij}^n - \frac{\mathbf{e}_{ij}^{n+1/2} \cdot \mathbf{F}_{ij}^C(r_{ij}^{n+1/2})}{\tau m_{ij}} \right] (e^{-\tau \Delta t} - 1) + \frac{\sigma \omega^R(r_{ij}^{n+1/2})}{m_{ij}} \sqrt{\frac{1 - e^{-2\tau \Delta t}}{2\tau}} \mathbf{R}_{ij}^n, \quad (34)$$

where $\tau = \gamma \omega^D(r_{ij}^{n+1/2}) / m_{ij}$.

Step 3: for each particle i ,

$$\mathbf{q}_i^{n+1} = \mathbf{q}_i^{n+1/2} + (\Delta t/2) m_i^{-1} \mathbf{p}_i^{n+1}. \quad (35)$$

In the same language, the so-called DPD-Trotter method [11, 46] would be equivalent to SAS where each interacting pair in the S part is also solved exactly in a successive manner as described above. We have observed in [11, 34] that the performance of DPD-Trotter is very similar to that of DPD-S1, therefore, we will not include the former for comparisons in the current article.

2.4 The ABOBA method

We can see from (27) that as we increase the value of the friction coefficient, the influence of the conservative force becomes less and less in the ASA method (30) in the previous section—in the limit of $\gamma \rightarrow \infty$, the ASA method effectively corresponds to the integration of an ideal gas (sometimes termed “ideal DPD fluid” within the DPD framework [59]). However, the conservative force plays a crucial role in guiding the movements of the particles. Therefore, as in the DPD-S1 method in Section 2.2, it may be more desirable to split the S part in the ASA method into B and O parts especially we are interested in the high friction limit in order to achieve a fluid-like Schmidt number (see more discussions in Section 1.2). Unlike the DPD-S1 method where the BBK method is used, each interacting pair in the O part (20) can be solved exactly by setting $F_{ij}^C = 0$ in the derivations in (26)–(29) in the previous section. In what follows we propose another new method, which we term the ABOBA method, whose propagator can be written as

$$\exp\left(\Delta t \hat{\mathcal{L}}_{\text{ABOBA}}\right) = \exp\left(\frac{\Delta t}{2} \mathcal{L}_A\right) \exp\left(\frac{\Delta t}{2} \mathcal{L}_B\right) \exp\left(\Delta t \hat{\mathcal{L}}_O\right) \exp\left(\frac{\Delta t}{2} \mathcal{L}_B\right) \exp\left(\frac{\Delta t}{2} \mathcal{L}_A\right), \quad (36)$$

where the propagation of the O part is similarly defined as in (31) with $F_{ij}^C = 0$. (It is also similar to (20) except each interacting pair is exactly solved.) Note that one may wish to reverse the order of the interacting pairs in the O part (or the S part in the ASA method (30)), which will not affect the order of convergence to the invariant measure (see more discussions in Section 2.5). The detailed integration steps of the ABOBA method read:

Step 1: for each particle i ,

$$\mathbf{q}_i^{n+1/2} = \mathbf{q}_i^n + (\Delta t/2) m_i^{-1} \mathbf{p}_i^n, \quad (37)$$

$$\mathbf{p}_i^{n+1/3} = \mathbf{p}_i^n + (\Delta t/2) \mathbf{F}_i^C(\mathbf{q}^{n+1/2}), \quad (38)$$

Step 2: for each interacting pair within cutoff radius ($r_{ij} < r_c$), in a successive manner,

$$\mathbf{p}_i^{n+2/3} = \mathbf{p}_i^{n+1/3} + m_{ij} \Delta v_{ij} \mathbf{e}_{ij}^{n+1/2}, \quad (39a)$$

$$\mathbf{p}_j^{n+2/3} = \mathbf{p}_j^{n+1/3} - m_{ij} \Delta v_{ij} \mathbf{e}_{ij}^{n+1/2}, \quad (39b)$$

with

$$\Delta v_{ij} = \left[\mathbf{e}_{ij}^{n+1/2} \cdot \mathbf{v}_{ij}^{n+1/3} \right] (e^{-\tau \Delta t} - 1) + \frac{\sigma \omega^R(r_{ij}^{n+1/2})}{m_{ij}} \sqrt{\frac{1 - e^{-2\tau \Delta t}}{2\tau}} \mathbf{R}_{ij}^n, \quad (40)$$

where $\tau = \gamma \omega^D(r_{ij}^{n+1/2})/m_{ij}$.

Step 3: for each particle i ,

$$\mathbf{p}_i^{n+1} = \mathbf{p}_i^{n+2/3} + (\Delta t/2) \mathbf{F}_i^C(\mathbf{q}^{n+1/2}), \quad (41)$$

$$\mathbf{q}_i^{n+1} = \mathbf{q}_i^{n+1/2} + (\Delta t/2) m_i^{-1} \mathbf{p}_i^{n+1}. \quad (42)$$

Note that the conservative force \mathbf{F}_i^C needs to be computed only once in (38), where the Verlet neighbor lists are also updated. The interacting pairs needed in the subsequent step can then be easily identified from the lists. Note also that if we switch off the O part, the ABOBA method reduces to the position Verlet method [40] for the Hamiltonian part where again A and B parts are solved exactly.

2.5 Accuracy of equilibrium averages

The framework of long-time Talay–Tubaro expansion has been widely used in the analysis of the accuracy of ergodic averages (with respect to the invariant measure) in stochastic numerical methods [1, 2, 12, 28–31, 35, 56]. In what follows we adopt the procedures to examine the order of convergence to the invariant measure of the methods described in Sections 2.2–2.4.

For a given splitting method described by $\mathcal{L} = \mathcal{L}_\alpha + \mathcal{L}_\beta + \dots + \mathcal{L}_\zeta$, we define its associated effective operator $\hat{\mathcal{L}}^\dagger$ with stepsize Δt as

$$\exp(\Delta t \hat{\mathcal{L}}^\dagger) = \exp(\Delta t \mathcal{L}_\alpha^\dagger) \exp(\Delta t \mathcal{L}_\beta^\dagger) \dots \exp(\Delta t \mathcal{L}_\zeta^\dagger), \quad (43)$$

where $\mathcal{L}_\alpha^\dagger, \mathcal{L}_\beta^\dagger, \dots, \mathcal{L}_\zeta^\dagger$ represent the corresponding Fokker–Planck operator associated with each subsystem. The effective operator $\hat{\mathcal{L}}^\dagger$ can be viewed as a perturbation of the exact Fokker–Planck operator $\mathcal{L}^\dagger = \mathcal{L}_\alpha^\dagger + \mathcal{L}_\beta^\dagger + \dots + \mathcal{L}_\zeta^\dagger$ for the whole system:

$$\hat{\mathcal{L}}^\dagger = \mathcal{L}^\dagger + \Delta t \mathcal{L}_1^\dagger + \Delta t^2 \mathcal{L}_2^\dagger + O(\Delta t^3), \quad (44)$$

where perturbation operators $\mathcal{L}_1^\dagger, \mathcal{L}_2^\dagger, \dots$ can be computed by using the Baker–Campbell–Hausdorff (BCH) expansion [20, 32]. We also define the perturbed invariant measure $\hat{\rho}$ associated with the numerical method as an approximation of the target invariant measure ρ_β :

$$\hat{\rho} = \rho_\beta [1 + \Delta t f_1 + \Delta t^2 f_2 + \Delta t^3 f_3 + O(\Delta t^4)], \quad (45)$$

where f_1, f_2, \dots are some correction functions. The average of each of those functions with respect to the target invariant measure is zero, i.e., $\langle f_i \rangle = 0$. Subsequently, substituting $\hat{\mathcal{L}}^\dagger$ and $\hat{\rho}$ into the stationary Fokker–Planck equation

$$\hat{\mathcal{L}}^\dagger \hat{\rho} = 0 \quad (46)$$

yields

$$[\mathcal{L}^\dagger + \Delta t \mathcal{L}_1^\dagger + \Delta t^2 \mathcal{L}_2^\dagger + O(\Delta t^3)] (\rho_\beta [1 + \Delta t f_1 + \Delta t^2 f_2 + \Delta t^3 f_3 + O(\Delta t^4)]) = 0. \quad (47)$$

Since the exact Fokker–Planck operator preserves the target invariant measure, i.e., $\mathcal{L}^\dagger \rho_\beta = 0$, we obtain

$$\mathcal{L}^\dagger(\rho_\beta f_1) = -\mathcal{L}_1^\dagger \rho_\beta \quad (48)$$

by equating first order terms in Δt . Although we are able to compute the perturbation operator \mathcal{L}_1^\dagger by using the BCH expansion for any particular splitting method, and subsequently its action on ρ_β , it is generally very hard to solve the above PDE (48) in order to obtain the leading correction function f_1 in closed form (see examples in Langevin dynamics [28] and adaptive Langevin dynamics [35]).

According to the BCH expansion, for (noncommutative) operators X and Y , we have

$$\exp(\Delta t X) \exp(\Delta t Y) = \exp(\Delta t Z_1), \quad (49)$$

where

$$Z_1 = X + Y + \frac{\Delta t}{2} [X, Y] + \frac{\Delta t^2}{12} ([X, [X, Y]] - [Y, [X, Y]]) + O(\Delta t^3), \quad (50)$$

where $[X, Y] = XY - YX$ denotes the commutator of operators X and Y . Subsequently, we have

$$\exp\left(\frac{\Delta t}{2}X\right)\exp(\Delta tY)\exp\left(\frac{\Delta t}{2}X\right) = \exp(\Delta tZ_2), \quad (51)$$

where

$$Z_2 = X + Y + \frac{\Delta t^2}{12} \left([Y, [Y, X]] - \frac{1}{2} [X, [X, Y]] \right) + O(\Delta t^4). \quad (52)$$

Therefore, there typically exists a nonzero term, $\mathcal{L}_1^\dagger \propto [X, Y] \neq 0$, for nonsymmetric splitting methods, while the condition $\mathcal{L}_1^\dagger = 0$, which implies $f_1 = 0$, is automatically satisfied for symmetric splitting methods. Thus, for observables $\phi(\mathbf{q}, \mathbf{p})$, assuming the asymptotic expansion holds, the computed average associated with symmetric splitting methods would be of order two

$$\langle \phi \rangle_{\Delta t} = \langle \phi \rangle + \Delta t \langle \phi f_1 \rangle + \Delta t^2 \langle \phi f_2 \rangle + \dots = \langle \phi \rangle + O(\Delta t^2). \quad (53)$$

For certain nonsymmetric splitting methods (i.e., $f_1 \neq 0$), it is also possible that $\langle \phi f_1 \rangle = 0$ with certain observables, in which case second order convergence to the invariant measure is also achieved (see an example in [36]). It should be noted that if certain conditions are satisfied, higher order convergence to the invariant measure would also be possible as demonstrated in [1, 2].

2.5.1 The DPD-S1 method

It is more convenient to work with the adjoint of the perturbed generator associated with a particular splitting method. In the case of the DPD-S1 method (19), we have

$$\exp\left(\Delta t \hat{\mathcal{L}}_{\text{DPD-S1}}^\dagger\right) = \exp\left(\frac{\Delta t}{2} \mathcal{L}_B^\dagger\right) \exp\left(\Delta t \mathcal{L}_A^\dagger\right) \exp\left(\frac{\Delta t}{2} \mathcal{L}_B^\dagger\right) \exp\left(\Delta t \hat{\mathcal{L}}_O^\dagger\right), \quad (54)$$

where

$$\exp\left(\Delta t \hat{\mathcal{L}}_O^\dagger\right) = \exp\left(\Delta t \hat{\mathcal{L}}_{O_{1,2}}^\dagger\right) \exp\left(\Delta t \hat{\mathcal{L}}_{O_{1,3}}^\dagger\right) \dots \exp\left(\Delta t \hat{\mathcal{L}}_{O_{N-1,N}}^\dagger\right). \quad (55)$$

Notice the apparent reversal of the sequence of products, known as the “vertauschungssatz” [20]. With the help of the BCH expansion and (21), the effective operator associated with the O part can be computed as

$$\begin{aligned} \hat{\mathcal{L}}_O^\dagger &= \mathcal{L}_O^\dagger + \frac{\Delta t}{2} \left[\mathcal{L}_{O_{1,2}}^\dagger, \mathcal{L}_{O_{1,3}}^\dagger \right] + \frac{\Delta t}{2} \left[\mathcal{L}_{O_{1,2}}^\dagger + \mathcal{L}_{O_{1,3}}^\dagger, \mathcal{L}_{O_{1,4}}^\dagger \right] + \dots \\ &\quad + \frac{\Delta t}{2} \left[\mathcal{L}_{O_{1,2}}^\dagger + \mathcal{L}_{O_{1,3}}^\dagger + \dots + \mathcal{L}_{O_{N-2,N}}^\dagger, \mathcal{L}_{O_{N-1,N}}^\dagger \right] + O(\Delta t^2), \end{aligned} \quad (56)$$

and subsequently we can obtain the effective operator associated with the overall method:

$$\hat{\mathcal{L}}_{\text{DPD-S1}}^\dagger = \mathcal{L}_H^\dagger + \mathcal{L}_O^\dagger + \Delta t \mathcal{L}_{1,\text{DPD-S1}}^\dagger + O(\Delta t^2), \quad (57)$$

where $\mathcal{L}_H^\dagger = \mathcal{L}_A^\dagger + \mathcal{L}_B^\dagger$ and

$$\begin{aligned} \mathcal{L}_{1,\text{DPD-S1}}^\dagger &= \frac{1}{2} \left[\mathcal{L}_H^\dagger, \mathcal{L}_O^\dagger \right] + \frac{1}{2} \left[\mathcal{L}_{O_{1,2}}^\dagger, \mathcal{L}_{O_{1,3}}^\dagger \right] + \frac{1}{2} \left[\mathcal{L}_{O_{1,2}}^\dagger + \mathcal{L}_{O_{1,3}}^\dagger, \mathcal{L}_{O_{1,4}}^\dagger \right] + \dots \\ &\quad + \frac{1}{2} \left[\mathcal{L}_{O_{1,2}}^\dagger + \mathcal{L}_{O_{1,3}}^\dagger + \dots + \mathcal{L}_{O_{N-2,N}}^\dagger, \mathcal{L}_{O_{N-1,N}}^\dagger \right]. \end{aligned} \quad (58)$$

It can be easily shown that

$$\mathcal{L}_H^\dagger \rho_\beta = 0, \quad \mathcal{L}_{O_{i,j}}^\dagger \rho_\beta = 0, \quad (59)$$

and subsequently

$$\mathcal{L}_{1,DPD-S1}^\dagger \rho_\beta = 0. \quad (60)$$

Therefore, the associated leading correction function in (48) must be zero, i.e.,

$$f_{1,DPD-S1} = 0. \quad (61)$$

Given that higher order perturbations in (45) are not equal to zero in general, we have shown that the nonsymmetric DPD-S1 method has second order convergence to its invariant measure.

If each interacting pair in the OU process has been solved exactly, the resulting OBAB method can be similarly shown to have second order convergence to its invariant measure as the DPD-S1 method. Since both methods involve a second order symplectic Verlet method for the Hamiltonian part and other actions only on the OU process, we may refer to them as generalized geometric Langevin algorithms of order two (GLA-2) [7] in the context of stochastic momentum-conserving thermostats. It is worth emphasizing that the OU process in stochastic momentum-conserving thermostats is pairwise and thus different from the standard setting of Langevin dynamics. Nevertheless, it has been demonstrated that second order convergence can also be achieved by the combination of a second order symplectic method for the Hamiltonian part and a second order method (or an exact solver) for the OU process (see more discussions on the long-time accuracy of the GLA-type methods in Langevin dynamics in [2, 7, 31]).

2.5.2 The ASA method

In the ASA method (30), we have

$$\exp(\Delta t \hat{\mathcal{L}}_{ASA}^\dagger) = \exp\left(\frac{\Delta t}{2} \mathcal{L}_A^\dagger\right) \exp(\Delta t \hat{\mathcal{L}}_S^\dagger) \exp\left(\frac{\Delta t}{2} \mathcal{L}_A^\dagger\right), \quad (62)$$

where

$$\exp(\Delta t \hat{\mathcal{L}}_S^\dagger) = \exp(\Delta t \mathcal{L}_{S_{1,2}}^\dagger) \exp(\Delta t \mathcal{L}_{S_{1,3}}^\dagger) \dots \exp(\Delta t \mathcal{L}_{S_{N-1,N}}^\dagger). \quad (63)$$

The effective operator associated with the overall method can be obtained as

$$\hat{\mathcal{L}}_{ASA}^\dagger = \mathcal{L}_A^\dagger + \mathcal{L}_S^\dagger + \Delta t \mathcal{L}_{1,ASA}^\dagger + O(\Delta t^2), \quad (64)$$

where

$$\begin{aligned} \mathcal{L}_{1,ASA}^\dagger &= \frac{1}{2} [\mathcal{L}_{S_{1,2}}^\dagger, \mathcal{L}_{S_{1,3}}^\dagger] + \frac{1}{2} [\mathcal{L}_{S_{1,2}}^\dagger + \mathcal{L}_{S_{1,3}}^\dagger, \mathcal{L}_{S_{1,4}}^\dagger] + \dots \\ &\quad + \frac{1}{2} [\mathcal{L}_{S_{1,2}}^\dagger + \mathcal{L}_{S_{1,3}}^\dagger + \dots + \mathcal{L}_{S_{N-2,N}}^\dagger, \mathcal{L}_{S_{N-1,N}}^\dagger]. \end{aligned} \quad (65)$$

For interacting pairs, i and j ($j > i$), and, k and l ($l > k$), we have

$$[\mathcal{L}_{S_{i,j}}^\dagger, \mathcal{L}_{S_{k,l}}^\dagger] \rho_\beta = \beta \rho_\beta \left(\mathcal{L}_{O_{i,j}}^\dagger (\mathbf{F}_{kl}^C(r_{kl}) \cdot \mathbf{v}_{kl}) - \mathcal{L}_{O_{k,l}}^\dagger (\mathbf{F}_{ij}^C(r_{ij}) \cdot \mathbf{v}_{ij}) \right), \quad (66)$$

which is nonzero if either of i and j is equal to either of k and l . Therefore, it can be seen from (65) that in general

$$\mathcal{L}_{1,ASA}^\dagger \rho_\beta \neq 0. \quad (67)$$

Therefore, the associated leading correction function in (48) is generally nonzero, i.e.,

$$f_{1,\text{ASA}} \neq 0. \quad (68)$$

Thus, unlike the DPD-S1 method, only first order convergence to its invariant measure is generally expected for the nonsymmetric ASA method.

In order to ensure second order convergence, one may modify the ASA method to be an ASSA-like method where notably the order of the interacting pairs in either of the S part needs to be reversed—the resulting method would be symmetric. However, in our numerical experiments we observed that the performance of the ASSA method was not as good as that of the ASA method with a friction coefficient of $\gamma = 4.5$ where the latter outperformed all other methods tested in Section 3. Note that the order of the interacting pairs in one of the S parts was suggested to be reversed in the symmetric DPD-Trotter (SAS) method [11, 46] mentioned at the end of Section 2.3, thereby ensuring second order convergence. Nevertheless, we observed that the performance of the DPD-Trotter (SAS) method was almost the same if the order was not reversed.

2.5.3 The ABOBA method

In the ABOBA method (36), we have

$$\exp\left(\Delta t \hat{\mathcal{L}}_{\text{ABOBA}}^\dagger\right) = \exp\left(\frac{\Delta t}{2} \mathcal{L}_A^\dagger\right) \exp\left(\frac{\Delta t}{2} \mathcal{L}_B^\dagger\right) \exp\left(\Delta t \hat{\mathcal{L}}_O^\dagger\right) \exp\left(\frac{\Delta t}{2} \mathcal{L}_B^\dagger\right) \exp\left(\frac{\Delta t}{2} \mathcal{L}_A^\dagger\right), \quad (69)$$

where

$$\exp\left(\Delta t \hat{\mathcal{L}}_O^\dagger\right) = \exp\left(\Delta t \mathcal{L}_{O_{1,2}}^\dagger\right) \exp\left(\Delta t \mathcal{L}_{O_{1,3}}^\dagger\right) \dots \exp\left(\Delta t \mathcal{L}_{O_{N-1,N}}^\dagger\right). \quad (70)$$

The effective operator associated with the overall method can be obtained as

$$\hat{\mathcal{L}}_{\text{ABOBA}}^\dagger = \mathcal{L}_A^\dagger + \mathcal{L}_B^\dagger + \mathcal{L}_O^\dagger + \Delta t \mathcal{L}_{1,\text{ABOBA}}^\dagger + O(\Delta t^2), \quad (71)$$

where

$$\begin{aligned} \mathcal{L}_{1,\text{ABOBA}}^\dagger = & \frac{1}{2} \left[\mathcal{L}_{O_{1,2}}^\dagger, \mathcal{L}_{O_{1,3}}^\dagger \right] + \frac{1}{2} \left[\mathcal{L}_{O_{1,2}}^\dagger + \mathcal{L}_{O_{1,3}}^\dagger, \mathcal{L}_{O_{1,4}}^\dagger \right] + \dots \\ & + \frac{1}{2} \left[\mathcal{L}_{O_{1,2}}^\dagger + \mathcal{L}_{O_{1,3}}^\dagger + \dots + \mathcal{L}_{O_{N-2,N}}^\dagger, \mathcal{L}_{O_{N-1,N}}^\dagger \right]. \end{aligned} \quad (72)$$

It can be easily shown that

$$\mathcal{L}_{1,\text{ABOBA}}^\dagger \rho_\beta = 0. \quad (73)$$

Therefore, the associated leading correction function in (48) must be zero, i.e.,

$$f_{1,\text{ABOBA}} = 0. \quad (74)$$

Thus, like the DPD-S1 method, second order convergence to its invariant measure is generally expected for the nonsymmetric ABOBA method.

3 Numerical experiments

In this section, a variety of numerical experiments are conducted to systematically compare the newly proposed ASA and ABOBA methods with alternative popular methods described in Section 2.

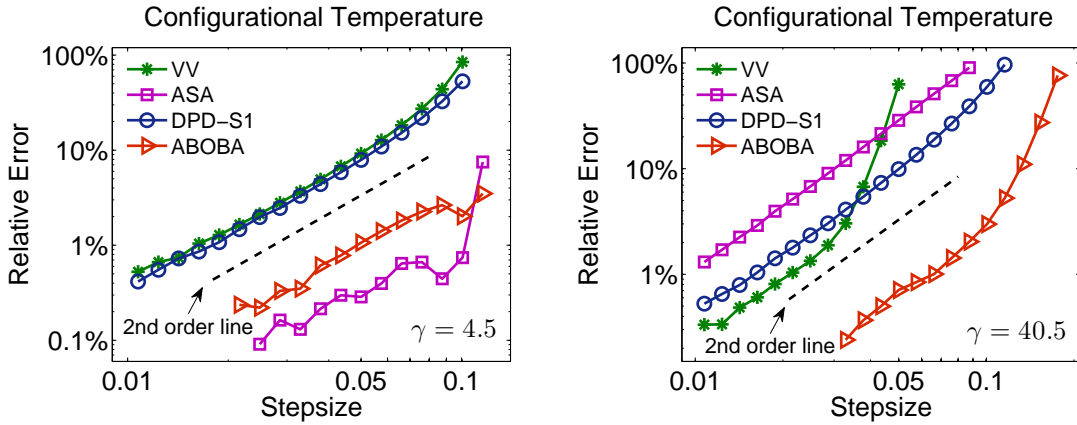


Figure 1: Double logarithmic plot of the relative error in the computed configurational temperature (75) against stepsize by using various numerical methods of the DPD system described in Section 2 with friction coefficients of $\gamma = 4.5$ (left) and $\gamma = 40.5$ (right). The system was simulated for 1000 reduced time units but only the last 80% of the data were collected to calculate the static quantity in order to make sure the system was well equilibrated. Ten different runs were averaged to reduce the sampling errors. The stepsizes tested began at around $\Delta t = 0.01$ and were increased incrementally by 15% until all methods either started to show significant relative errors or became unstable (e.g., the VV method on the right panel at slightly over $\Delta t = 0.05$). The dashed black line represents the second order convergence to the invariant measure.

3.1 Simulation details

In our numerical experiments, we adopted a standard set of parameters commonly used in algorithms tests as in [3, 19]. Specifically, particle mass m_i , cutoff radius r_c , and $k_B T$ were set to be unity. Although a particle density of $\rho_d = 4$ was initially used in [19] and later adopted in a number of studies [42, 51, 59], a smaller value of $\rho_d = 3$ was later suggested for efficiency reasons and thus was used throughout the current article. Subsequently, a repulsion parameter of $a_{ij} = 75k_B T/\rho_d = 25$ was determined in order to match the compressibility of water [19]. Although a friction coefficient of $\gamma = 4.5$ was widely used in algorithms tests, the corresponding Schmidt number was only $Sc \approx 0.6$ according to (10)—a gas-like Schmidt number (see more discussions in Section 1.2). While larger value of $\gamma = 40.5$, which corresponds to $Sc \approx 8.7$, was examined in [34, 36], even larger values of the friction coefficient are needed to have fluid-like Schmidt numbers. Therefore, we also included friction coefficients of $\gamma = 200$ and $\gamma = 450$, corresponding to Schmidt numbers of $Sc \approx 201$ and $Sc \approx 1016$, respectively.

Moreover, a system of $N = 500$ identical particles was simulated in a cubic box with periodic boundary conditions [5, 17]. While the initial positions of the particles were independent and identically distributed (i.i.d.) with a uniform distribution over the box, the initial momenta were i.i.d. normal random variables with mean zero and variance $k_B T$. Verlet neighbor lists [60] were used wherever possible in order to reduce the computational cost as discussed in Section 2.

Following [34, 36], we measured the “numerical efficiency”, defined as the ratio of the “critical stepsize” and the CPU time per step, of each method and then scaled it to that of the benchmark VV method, unless otherwise stated. The CPU time (in milliseconds) for the main integration steps (without calculating any physical quantities) was the time

Method	Critical stepsize	CPU time	Scaled efficiency
VV	0.016	6.829	100.0%
ASA	0.101	6.652	648.1%
DPD-S1	0.019	7.852	103.3%
ABOBA	0.050	7.742	275.7%

Table 1: Comparisons of the “numerical efficiency” of various numerical methods of the DPD system with a friction coefficient of $\gamma = 4.5$. “Critical stepsize” is the stepsize beyond which the numerical method starts to show pronounced artifacts (i.e., 1% relative error in the computed configurational temperature according to the left panel of Figure 1). The numerical efficiency of each method was scaled to that of the benchmark VV method.

Method	Critical stepsize	CPU time	Scaled efficiency
VV	0.022	6.829	100.0%
ASA	0.010	6.652	46.7%
DPD-S1	0.016	7.852	63.3%
ABOBA	0.066	7.742	264.6%

Table 2: Comparisons of the “numerical efficiency” of various numerical methods of the DPD system with a large friction coefficient of $\gamma = 40.5$, corresponding to the right panel of Figure 1. The format of the table is the same as in Table 1.

taken (on a Lenovo ThinkStation P330 Tiny) for the integration of a single time step of $\Delta t = 0.05$ (averaged over 10,000 consecutive time steps). Note that Verlet neighbor lists [60] were again used wherever possible. The critical stepsize was determined as the stepsize that corresponds to a 1% relative error in the computed configurational temperature [3, 8, 44, 58], an observable function that depends solely on the positions. Moreover, the average of the computed configurational temperature in the canonical ensemble is expected to be precisely the target temperature:

$$k_B T = \frac{\langle \nabla_i U(\mathbf{q}) \cdot \nabla_i U(\mathbf{q}) \rangle}{\langle \nabla_i^2 U(\mathbf{q}) \rangle}, \quad (75)$$

where $\nabla_i U$ and $\nabla_i^2 U$ respectively represent the gradient and Laplacian of the potential energy U with respect to the position of particle i (see more discussions on the configurational temperature in [34, 36]). It should be noted that since the canonical momentum distribution is always Gaussian (and thus trivial to sample), as in Langevin dynamics [30] we are far more interested in sampling configurational quantities. Thus the configurational temperature (75) was chosen over the kinetic temperature that depends solely on the momenta. Importantly, good control of the configurational temperature appears to imply good performance in other physical quantities tested in Section 3 (see more discussions on the reasoning in [34]). Moreover, it has been recommended in [3] that the configurational temperature (75), as a verification of equilibrium, should be measured and reported in DPD simulations.

In addition, we calculated the radial distribution function (RDF) [5, 17], often denoted as $g(r)$, which is another important configurational quantity in simulations, characterizing the structure of the system. Moreover, we also included the (normalized) velocity autocorrelation

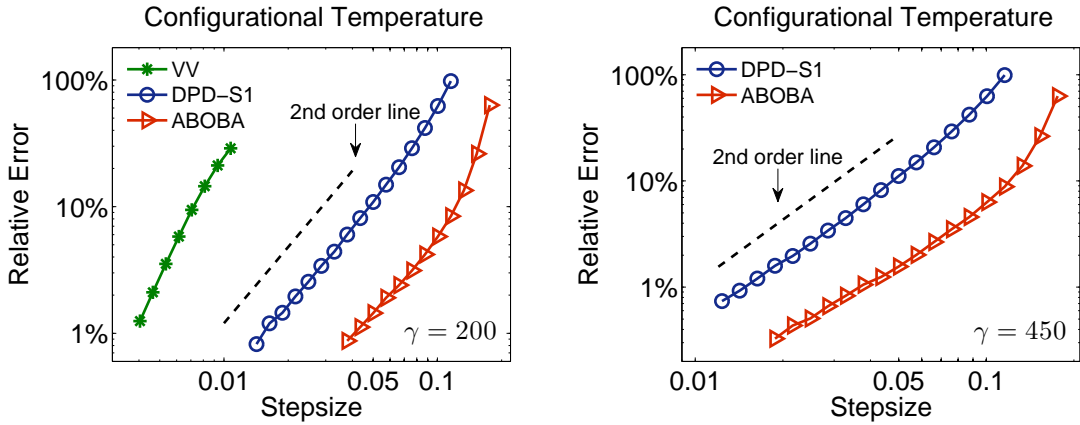


Figure 2: Comparisons of the relative error in the computed configurational temperature against stepsize by using various numerical methods of the DPD system with friction coefficients of $\gamma = 200$ (left) and $\gamma = 450$ (right). The format of the plots is the same as in Figure 1. Note that the VV method on the left panel became unstable at slightly over $\Delta t = 0.01$.

Method	Critical stepsize	CPU time	Scaled efficiency
VV	0.004	6.829	100.0%
DPD-S1	0.015	7.852	326.1%
ABOBA	0.040	7.742	882.1%

Table 3: Comparisons of the “numerical efficiency” of various numerical methods of the DPD system with a very large friction coefficient of $\gamma = 200$, corresponding to the left panel of Figure 2. The format of the table is the same as in Table 1.

function (VAF) defined as

$$\psi(t) = \frac{\langle \mathbf{v}_i(t) \cdot \mathbf{v}_i(0) \rangle}{\langle \mathbf{v}_i(0) \cdot \mathbf{v}_i(0) \rangle}, \quad (76)$$

where $\mathbf{v}_i(0)$ is the initial velocity of particle i picked up after the system is well equilibrated. The VAF characterizes the translational diffusion of the system, thereby serving as an important measure of dynamical fidelity that numerical methods should be able to reproduce. Note that although (76) does not depend on the positions, the integral of an unnormalized VAF relates to the translational diffusion coefficient (i.e., the Green–Kubo relations [18, 25]), which can be alternatively measured by means of the mean squared displacement that indeed depends on the positions (see more discussions in [10]).

3.2 Numerical results

The configurational temperature control for a variety of methods described in Section 2 was compared in Figure 1. According to the dashed order line on both panels, we can see that all the methods tested exhibit second order convergence to the invariant measure, although only first order was expected for the VV and ASA methods. Note that in some cases the errors appear to grow more rapidly when approaching their respective stability thresholds—notably the VV method on the right panel became unstable at slightly over $\Delta t = 0.05$.

Method	Critical stepsize	CPU time	Scaled efficiency
DPD-S1	0.016	7.852	100.0%
ABOBA	0.038	7.742	240.9%

Table 4: Comparisons of the “numerical efficiency” of the DPD-S1 and ABOBA methods of the DPD system with an extremely large friction coefficient of $\gamma = 450$, corresponding to the right panel of Figure 2. The format of the table is the same as in Table 1 except the numerical efficiency of ABOBA was scaled to that of DPD-S1.

More specifically, in the friction limit of $\gamma = 4.5$ on the left panel of Figure 1, the DPD-S1 method is only marginally better than the VV method. Remarkably, the newly proposed ABOBA method achieves about one order of magnitude improvement over both methods in terms of the numerical accuracy for a fixed stepsize, while another newly proposed method of ASA is even more accurate. The substantial improvements of ABOBA and ASA are quantified by measuring the numerical efficiency with a fixed level of accuracy in Table 1, showing that ABOBA achieves a more than 170% improvement over the benchmark VV method while ASA remarkably has an almost 550% enhancement. Note that a 100% improvement in the numerical efficiency effectively doubles the performance.

In dark contrast, ASA appears to be the least accurate method among those tested in the large friction limit of $\gamma = 40.5$ on the right panel of Figure 1. As discussed at the start of Section 2.4, ASA is not suitable for large friction coefficients, thus in what follows it will not be included in comparisons with larger friction coefficients. The DPD-S1 method is constantly more accurate than ASA, while the VV method slightly outperforms DPD-S1 until it starts to blow up just over $\Delta t = 0.03$. Moreover, the ABOBA method clearly outperforms all the other methods by at least one order of magnitude—Table 2 confirms that ABOBA achieves a more than 160% improvement in the numerical efficiency over the benchmark VV method, while both ASA and DPD-S1 have only about half the numerical efficiency of VV.

We also explore the performance of various methods with larger friction coefficients in Figure 2 where second order convergence to the invariant measure was again observed for all the methods tested except the VV method on the left panel, corresponding to the very large friction limit of $\gamma = 200$. As in the case of $\gamma = 40.5$, it is possible that the error appears to grow more rapidly as the VV method approaches its stability threshold just over $\Delta t = 0.01$. As a result, in what follows VV will not be included for the extremely large friction limit of $\gamma = 450$.

In the very large friction limit of $\gamma = 200$ on the left panel of Figure 2, with a fixed level of accuracy it can be easily seen that both DPD-S1 and ABOBA can use substantially larger stepsizes than that of VV. To be more precise according to Table 3, a stepsize almost four times as large as that of VV can be used for DPD-S1, contributing to a more than 220% improvement in the numerical efficiency, while a stepsize ten times as large can be used for ABOBA, leading to a remarkable more than 780% enhancement. In the extremely large friction limit of $\gamma = 450$ on the right panel, ABOBA again comfortably outperforms DPD-S1, with a more than 140% improvement according to Table 4.

Figure 3 compares the RDF that characterizes the structure of the DPD system with a friction coefficient of $\gamma = 4.5$. Both VV and DPD-S1 start to show pronounced artifacts at around $\Delta t = 0.09$ and the RDFs appear to be heavily destroyed at around $\Delta t = 0.13$ in

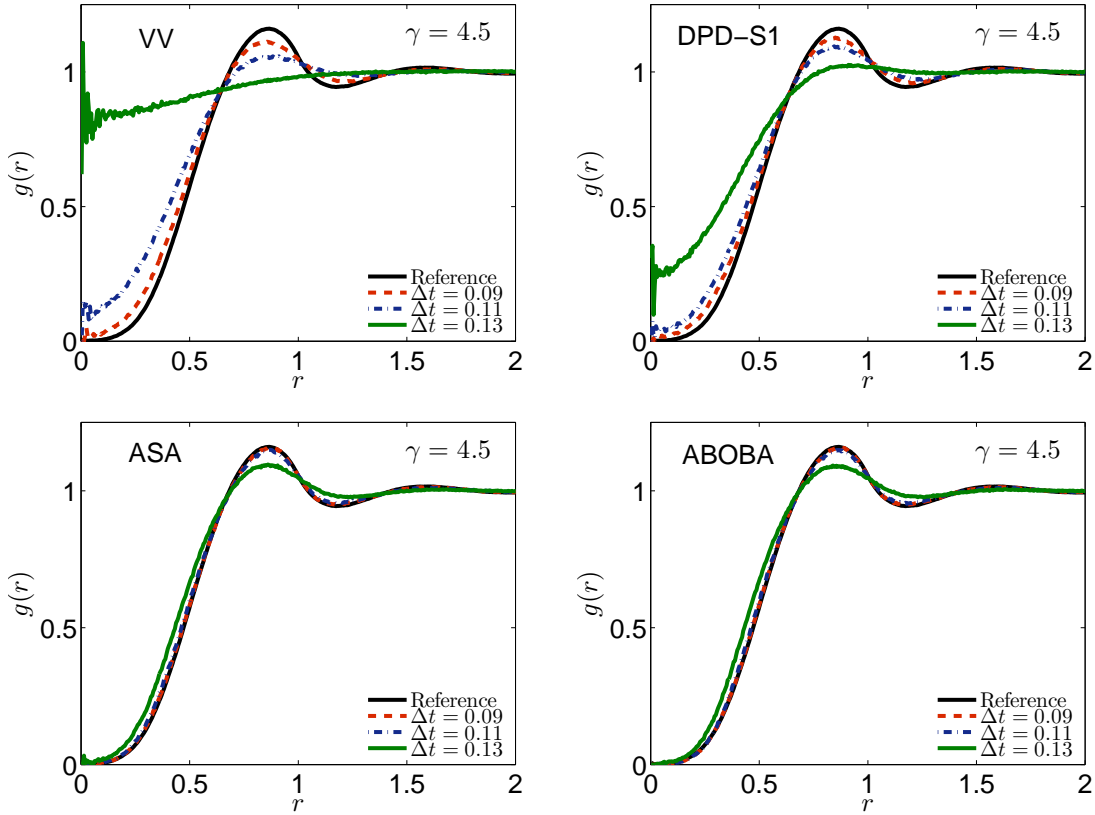


Figure 3: Comparisons of the radial distribution function (RDF), $g(r)$, obtained from various numerical methods of the DPD system with a friction coefficient of $\gamma = 4.5$. The solid black line is the reference solution obtained by using the DPD-S1 method with a very small stepsize of $\Delta t = 0.001$, while the colored lines correspond to different stepsizes as indicated.

both cases. Consistent with our findings on the left panel of Figure 1, larger stepsizes can be used for both ASA and ABOBA without compromising the control of the structure of the system—the RDFs are almost indistinguishable from the reference solution with a stepsize as large as $\Delta t = 0.11$, while only small deviations were observed in the RDFs with a stepsize of $\Delta t = 0.13$. It is worth pointing out that although ASA is more accurate in the configurational temperature control and has a much better numerical efficiency in Table 1 than ABOBA, its performance in controlling the RDF appears to be rather similar to that of ABOBA.

In the large friction limit of $\gamma = 40.5$ in Figure 4, the performance of various methods largely align with our observations on the right panel of Figure 1. Firstly, the VV method again became unstable at slightly over $\Delta t = 0.05$, at which point the RDF visibly deviates from the reference solution. Secondly, the joint best-performing ASA method in Figure 3 starts to show pronounced artifacts at only around $\Delta t = 0.05$. Finally, ABOBA again comfortably outperforms DPD-S1—while, with a stepsize of $\Delta t = 0.13$, the RDF of the former is almost indistinguishable from the reference solution, significant deviations can be observed from the latter.

Since the performance of the methods were very similar with friction coefficients of $\gamma = 200$ and $\gamma = 450$, only the results of the latter were included in Figure 5. Again consistent with

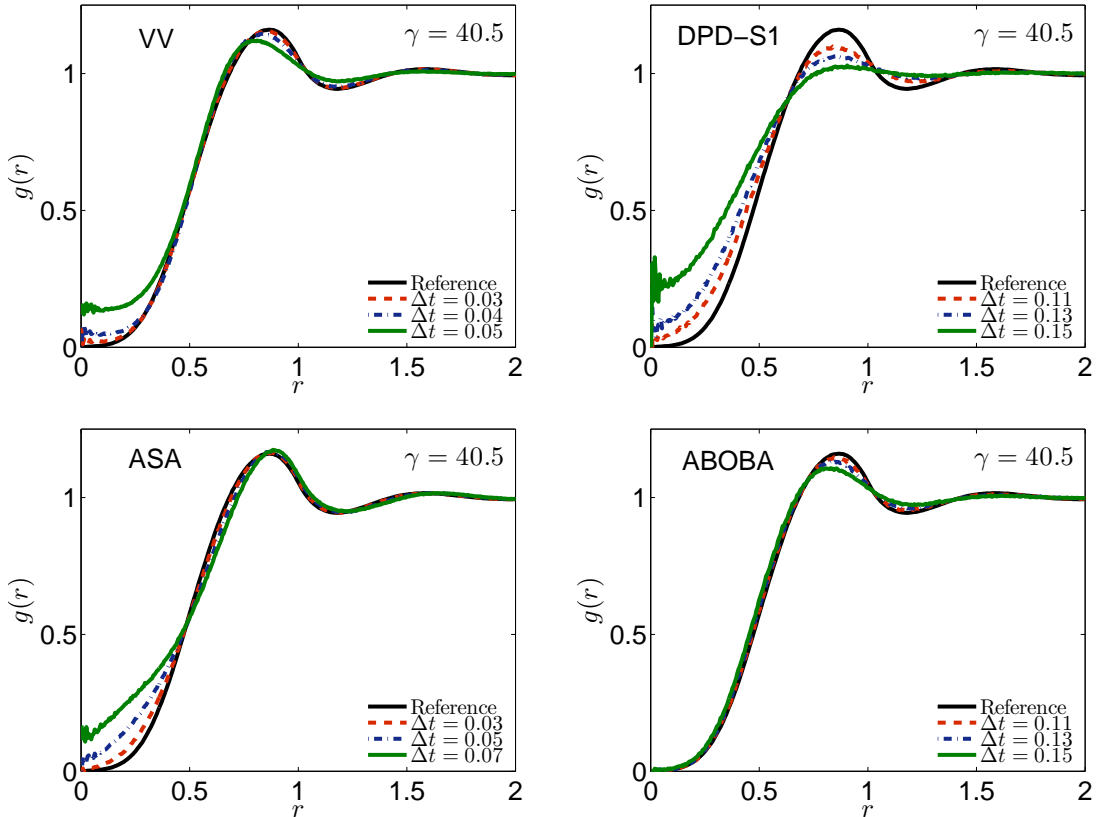


Figure 4: (Color.) Comparisons of the radial distribution function (RDF), $g(r)$, obtained from various numerical methods of the DPD system with a large friction coefficient of $\gamma = 40.5$. The format of the plots is the same as in Figure 3. Note that much smaller stepsizes were used in the VV and ASA methods.

our findings on the right panel of Figure 2, larger stepsizes can be used for ABOBA while maintaining good control of the structure of the system—while, with a stepsize of $\Delta t = 0.15$, the RDF of ABOBA shows rather small deviations from the reference solution, it is heavily destroyed for DPD-S1.

The control of the VAF (76), which characterizes dynamical properties of the DPD system, was also tested and plotted in Figure 6 with a friction coefficient of $\gamma = 4.5$. Consistent with our findings on the control of the configurational temperature on the left panel of Figure 1 and the RDF in Figure 3, both VV and DPD-S1 are outperformed by either ASA or ABOBA especially when stepsizes are relatively large. However, notably the differences are not as significant as in the other two quantities. Again as in Figure 3, despite its better control of the configurational temperature, the performance of ASA is very similar to that of ABOBA.

In the large friction limit of $\gamma = 40.5$ in Figure 7, the VV method again became unstable at slightly over $\Delta t = 0.05$, at which point, unlike in Figure 4, its VAF matches very well with the reference solution. While, with a stepsize of $\Delta t = 0.11$, the VAF of DPD-S1 clearly deviates from the reference solution, the performance of ABOBA appears to be much better, matching the reference solution reasonably well. Surprisingly, unlike in Figure 4, ASA performs almost

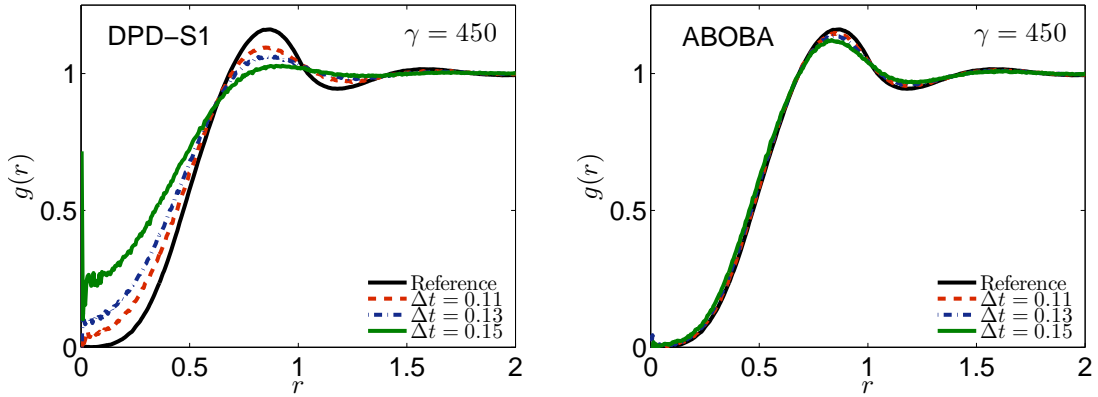


Figure 5: Comparisons of the radial distribution function (RDF), $g(r)$, obtained from the DPD-S1 method (left) and the ABOBA method (right) of the DPD system with an extremely large friction coefficient of $\gamma = 450$. The format of the plots is the same as in Figure 3.

as well as ABOBA. However, given its terrible performance in the RDF control as shown in Figure 4, the ASA method should not be preferred in the large friction limit of $\gamma = 40.5$ (and beyond). We would also like to mention that in the larger friction limits of $\gamma = 200$ and $\gamma = 450$ (results not shown) the ABOBA method also (slightly) outperforms the DPD-S1 method.

Given the fact that the BAOAB method is the best-performing method in terms of sampling configurational quantities in Langevin dynamics [28–30] (see also a recent comprehensive study on its time correlations [47]), it is worth mentioning that a BAOAB method in the DPD context can be easily constructed following the procedures in Section 2.4. However, it is crucial to note that in the DPD context, when updating the OU process in the BAOAB method, all the distances between (updated) interacting pairs have to be recalculated, the cost of which is essentially the same as another force calculation. In contrast, the recalculation can be easily avoided with the help of the Verlet neighbor lists in the ABOBA method. Therefore, unless at least twice as large stepsize can be used in BAOAB as that of ABOBA while maintaining the same level of accuracy in physical quantities of interest, the numerical efficiency of the former will be outperformed by the latter. We observed that the performance of BAOAB in terms of RDF and VAF is very similar to that of ABOBA. Although BAOAB is able to outperform ABOBA in the numerical efficiency in terms of the configurational temperature with friction coefficients of $\gamma = 200$ and $\gamma = 450$ if the level of accuracy required is low enough (e.g., less than 1%), overall we conclude that the ABOBA method should be preferred. It is also worth mentioning that a superconvergence (i.e., a fourth order convergence to the invariant measure) result observed only in the BAOAB method in the large friction limit in Langevin dynamics [28,31] (see another example in adaptive Langevin dynamics [35]) was not observed in the DPD context.

4 Conclusions

We have proposed two promising splitting methods of the DPD system, namely ASA and ABOBA, each of which relies on solving the splitting parts exactly. We have also demonstrated

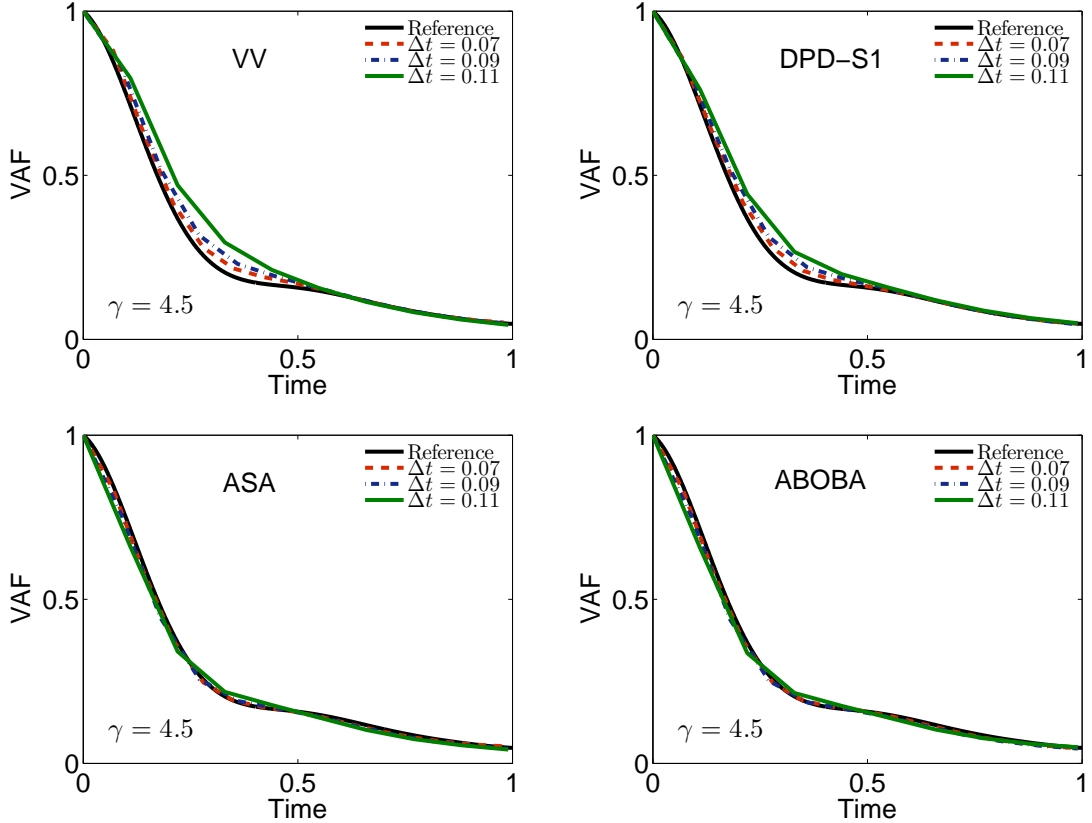


Figure 6: (Color.) Comparisons of the velocity autocorrelation function (VAF) (76) obtained from various numerical methods of the DPD system with a friction coefficient of $\gamma = 4.5$. Note that 100 different runs were averaged to reduce the sampling errors after the system was well equilibrated. The solid black line is the reference solution obtained by using the DPD-S1 method with a very small stepsize of $\Delta t = 0.001$, while the colored lines correspond to different stepsizes as indicated.

and numerically verified the second order convergence to the invariant measure for both DPD-S1 and ABOBA. Although only first order convergence was expected for both VV and ASA, both methods have exhibited second order convergence in our numerical experiments. While ASA substantially outperforms existing popular methods of VV and DPD-S1 with a friction coefficient of $\gamma = 4.5$, a standard choice in DPD simulations, it has been demonstrated that it is not suitable for (much) larger friction coefficients required for a fluid-like Schmidt number. Remarkably, ABOBA comfortably outperforms both VV and DPD-S1 with a wide range of the friction coefficients in all the physical quantities tested.

To be more precise, in terms of the configurational temperature control, ABOBA is at least one order of magnitude more accurate than the benchmark VV method with a fixed stepsize in each of the cases in Figures 1–2. Moreover, VV became unstable easily (slightly over $\Delta t = 0.05$ with $\gamma = 40.5$ and $\Delta t = 0.01$ with $\gamma = 200$) as the friction coefficient was increased, which indicates that vanishingly small stepsizes have to be used in the extremely large friction limit of $\gamma = 450$, effectively ruling it out especially for large-scale DPD simulations with a fluid-like Schmidt number. Furthermore, ABOBA constantly outperforms

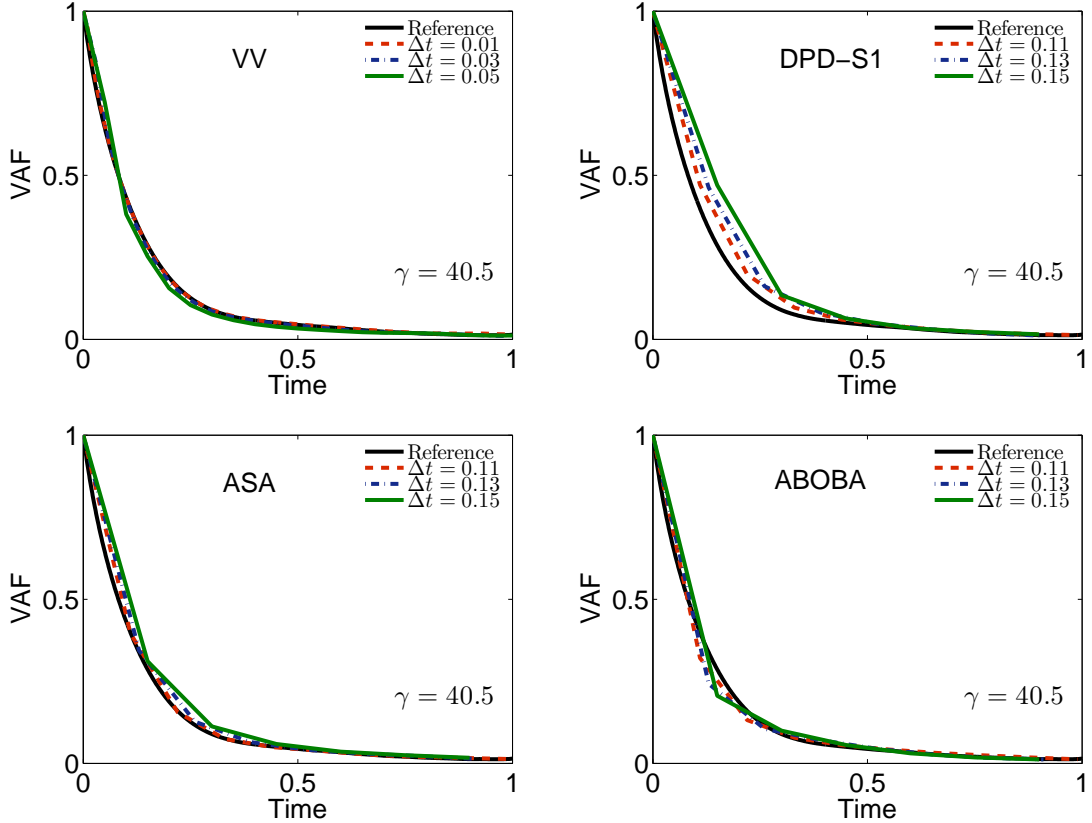


Figure 7: Comparisons of the velocity autocorrelation function (VAF) (76) obtained from various numerical methods of the DPD system with a large friction coefficient of $\gamma = 40.5$. The format of the plots is the same as in Figure 6. Note that much smaller stepsizes were used in the VV method.

the most recommended DPD-S1 method, achieving a more than 100% improvement (i.e., at least doubling the performance) in each of the cases in Tables 1–4. As previously mentioned, good control of the configurational temperature appears to lead to good performance in other physical quantities (with the sole exception of ASA in the VAF control in the large friction limit, where it is not that reliable). In all the comparisons of the RDF and VAF, ABOBA again can use larger stepsizes than that of DPD-S1 in order to maintain the same level of accuracy. This again illustrates the importance of optimal design of numerical methods.

Although the VV method has been substantially outperformed by the ABOBA method, the parallelization of the latter (along with ASA and DPD-S1), due to the fact that the interacting pairs in the OU process are solved successively, is not as straightforward as that of the former. However, a similar task of parallelizing the DPD-S1 method has been addressed by Larentzos et al. [26]—the procedures can be easily adopted for parallelizing both ABOBA and ASA.

Inspired by recent developments in adaptive thermostats [22, 35, 50] (their theoretical foundations have recently been taken up in [33]), the so-called pairwise adaptive Langevin (PAdL) thermostat has been proposed in [36]. PAdL is able to correct for thermodynamic observables while mimicking the dynamical properties of DPD and thus can be viewed as

“adaptive DPD”. It has been demonstrated in [36] that PAdL can also outperform popular numerical methods (including DPD-S1) for DPD in both equilibrium and nonequilibrium (driven by Lees–Edwards boundary conditions [27]) settings. Since PAdL is not based on the standard DPD formulation, it has not been included for comparisons in the current article. However, it will be interesting to compare its performance with the outstanding ABOBA method proposed in the current article. We leave further exploration of this direction for future work.

References

- [1] A. Abdulle, G. Vilmart, and K. C. Zygalakis. High order numerical approximation of the invariant measure of ergodic SDEs. *SIAM J. Numer. Anal.*, 52(4):1600–1622, 2014.
- [2] A. Abdulle, G. Vilmart, and K. C. Zygalakis. Long time accuracy of Lie–Trotter splitting methods for Langevin dynamics. *SIAM J. Numer. Anal.*, 53(1):1–16, 2015.
- [3] M. P. Allen. Configurational temperature in membrane simulations using dissipative particle dynamics. *J. Phys. Chem. B*, 110(8):3823–3830, 2006.
- [4] M. P. Allen and F. Schmid. A thermostat for molecular dynamics of complex fluids. *Mol. Simul.*, 33(1-2):21–26, 2007.
- [5] M. P. Allen and D. J. Tildesley. *Computer Simulation of Liquids*. Oxford University Press, 1989.
- [6] G. Besold, I. Vattulainen, M. Karttunen, and J. M. Polson. Towards better integrators for dissipative particle dynamics simulations. *Phys. Rev. E*, 62(6):R7611, 2000.
- [7] N. Bou-Rabee and H. Owhadi. Long-run accuracy of variational integrators in the stochastic context. *SIAM J. Numer. Anal.*, 48(1):278–297, 2010.
- [8] C. Braga and K. P. Travis. A configurational temperature Nosé–Hoover thermostat. *J. Chem. Phys.*, 123:134101, 2005.
- [9] A. Brünger, C. L. Brooks III, and M. Karplus. Stochastic boundary conditions for molecular dynamics simulations of ST2 water. *Chem. Phys. Lett.*, 105(5):495–500, 1984.
- [10] A. Chaudhri and J. R. Lukes. Velocity and stress autocorrelation decay in isothermal dissipative particle dynamics. *Phys. Rev. E*, 81(2):026707, 2010.
- [11] G. De Fabritiis, M. Serrano, P. Español, and P. V. Coveney. Efficient numerical integrators for stochastic models. *Phys. A*, 361(2):429–440, 2006.
- [12] A. Debussche and E. Faou. Weak backward error analysis for SDEs. *SIAM J. Numer. Anal.*, 50(3):1735–1752, 2012.
- [13] P. Español and P. Warren. Statistical mechanics of dissipative particle dynamics. *Europhys. Lett.*, 30(4):191, 1995.
- [14] P. Español and P. B. Warren. Perspective: Dissipative particle dynamics. *J. Chem. Phys.*, 146(15):150901, 2017.

- [15] X. Fan, N. Phan-Thien, S. Chen, X. Wu, and T. Y. Ng. Simulating flow of DNA suspension using dissipative particle dynamics. *Phys. Fluids*, 18(6):063102, 2006.
- [16] D. A. Fedosov, H. Noguchi, and G. Gompper. Multiscale modeling of blood flow: from single cells to blood rheology. *Biomech. Model. Mechanobiol.*, 13(2):239–258, 2013.
- [17] D. Frenkel and B. Smit. *Understanding Molecular Simulation: From Algorithms to Applications, Second Edition*. Academic Press, 2001.
- [18] M. S. Green. Markoff random processes and the statistical mechanics of time-dependent phenomena. II. Irreversible processes in fluids. *J. Chem. Phys.*, 22(3):398–413, 1954.
- [19] R. D. Groot and P. B. Warren. Dissipative particle dynamics: Bridging the gap between atomistic and mesoscopic simulation. *J. Chem. Phys.*, 107:4423, 1997.
- [20] E. Hairer, C. Lubich, and G. Wanner. *Geometric Numerical Integration: Structure-Preserving Algorithms for Ordinary Differential Equations*. Springer, 2006.
- [21] P. J. Hoogerbrugge and J. M. V. A. Koelman. Simulating microscopic hydrodynamic phenomena with dissipative particle dynamics. *Europhys. Lett.*, 19(3):155, 1992.
- [22] A. Jones and B. Leimkuhler. Adaptive stochastic methods for sampling driven molecular systems. *J. Chem. Phys.*, 135(8):084125, 2011.
- [23] P. E. Kloeden and E. Platen. *Numerical Solution of Stochastic Differential Equations*. Springer, 1992.
- [24] J. M. V. A. Koelman and P. J. Hoogerbrugge. Dynamic simulations of hard-sphere suspensions under steady shear. *Europhys. Lett.*, 21(3):363, 1993.
- [25] R. Kubo. Statistical-mechanical theory of irreversible processes. I. General theory and simple applications to magnetic and conduction problems. *J. Phys. Soc. Jpn.*, 12(6):570–586, 1957.
- [26] J. P. Larentzos, J. K. Brennan, J. D. Moore, M. Lísal, and W. D. Mattson. Parallel implementation of isothermal and isoenergetic dissipative particle dynamics using Shardlow-like splitting algorithms. *Comput. Phys. Commun.*, 185(7):1987–1998, 2014.
- [27] A. W. Lees and S. F. Edwards. The computer study of transport processes under extreme conditions. *J. Phys. C: Solid State Phys.*, 5(15):1921, 1972.
- [28] B. Leimkuhler and C. Matthews. Rational construction of stochastic numerical methods for molecular sampling. *Appl. Math. Res. Express*, 2013(1):34–56, 2013.
- [29] B. Leimkuhler and C. Matthews. Robust and efficient configurational molecular sampling via Langevin dynamics. *J. Chem. Phys.*, 138:174102, 2013.
- [30] B. Leimkuhler and C. Matthews. *Molecular Dynamics: With Deterministic and Stochastic Numerical Methods*. Springer, 2015.

- [31] B. Leimkuhler, C. Matthews, and G. Stoltz. The computation of averages from equilibrium and nonequilibrium Langevin molecular dynamics. *IMA J. Numer. Anal.*, 36(1):13–79, 2016.
- [32] B. Leimkuhler and S. Reich. *Simulating Hamiltonian Dynamics*. Cambridge University Press, 2005.
- [33] B. Leimkuhler, M. Sachs, and G. Stoltz. Hypercoercivity properties of adaptive Langevin dynamics. *arXiv:1908.09363*, 2019.
- [34] B. Leimkuhler and X. Shang. On the numerical treatment of dissipative particle dynamics and related systems. *J. Comput. Phys.*, 280:72–95, 2015.
- [35] B. Leimkuhler and X. Shang. Adaptive thermostats for noisy gradient systems. *SIAM J. Sci. Comput.*, 38(2):A712–A736, 2016.
- [36] B. Leimkuhler and X. Shang. Pairwise adaptive thermostats for improved accuracy and stability in dissipative particle dynamics. *J. Comput. Phys.*, 324:174–193, 2016.
- [37] M. Lísal, J. K. Brennan, and J. B. Avalos. Dissipative particle dynamics at isothermal, isobaric, isoenergetic, and isoenthalpic conditions using Shardlow-like splitting algorithms. *J. Chem. Phys.*, 135(20):204105, 2011.
- [38] S. Litvinov, M. Ellero, X. Hu, and N. Adams. A splitting scheme for highly dissipative smoothed particle dynamics. *J. Comput. Phys.*, 229(15):5457–5464, 2010.
- [39] C. P. Lowe. An alternative approach to dissipative particle dynamics. *Europhys. Lett.*, 47(2):145, 1999.
- [40] S. Melchionna. Design of quasisymplectic propagators for Langevin dynamics. *J. Chem. Phys.*, 127:044108, 2007.
- [41] E. Moeendarbary, T. Y. Ng, and M. Zangeneh. Dissipative particle dynamics: Introduction, methodology and complex fluid applications – a review. *Int. J. Appl. Mech.*, 1(04):737–763, 2009.
- [42] P. Nikunen, M. Karttunen, and I. Vattulainen. How would you integrate the equations of motion in dissipative particle dynamics simulations? *Comput. Phys. Commun.*, 153(3):407–423, 2003.
- [43] S. Plimpton. Fast parallel algorithms for short-range molecular dynamics. *J. Comput. Phys.*, 117(1):1–19, 1995.
- [44] H. H. Rugh. Dynamical approach to temperature. *Phys. Rev. Lett.*, 78(5):772, 1997.
- [45] M. A. Seaton, R. L. Anderson, S. Metz, and W. Smith. DL-MESO: highly scalable mesoscale simulations. *Mol. Simul.*, 39(10):796–821, 2013.
- [46] M. Serrano, G. De Fabritiis, P. Español, and P. V. Coveney. A stochastic Trotter integration scheme for dissipative particle dynamics. *Math. Comput. Simulation*, 72(2):190–194, 2006.

- [47] X. Shang and M. Kröger. Time correlation functions of equilibrium and nonequilibrium Langevin dynamics: Derivations and numerics using random numbers. *SIAM Rev.*, 2020.
- [48] X. Shang, M. Kröger, and B. Leimkuhler. Assessing numerical methods for molecular and particle simulation. *Soft Matter*, 13:8565–8578, 2017.
- [49] X. Shang and H. C. Öttinger. Structure-preserving integrators for dissipative systems based on reversible–irreversible splitting. *Proc. R. Soc. A*, 476(2234):20190446, 2018.
- [50] X. Shang, Z. Zhu, B. Leimkuhler, and A. J. Storkey. Covariance-controlled adaptive Langevin thermostat for large-scale Bayesian sampling. In *Advances in Neural Information Processing Systems 28*, pages 37–45. Curran Associates, 2015.
- [51] T. Shardlow. Splitting for dissipative particle dynamics. *SIAM J. Sci. Comput.*, 24(4):1267–1282, 2003.
- [52] T. Shardlow and Y. Yan. Geometric ergodicity for dissipative particle dynamics. *Stoch. Dyn.*, 6(01):123–154, 2006.
- [53] T. Soddeemann, B. Dünweg, and K. Kremer. Dissipative particle dynamics: A useful thermostat for equilibrium and nonequilibrium molecular dynamics simulations. *Phys. Rev. E*, 68(4):046702, 2003.
- [54] N. A. Spenley. Scaling laws for polymers in dissipative particle dynamics. *Europhys. Lett.*, 49(4):534–540, 2000.
- [55] S. D. Stoyanov and R. D. Groot. From molecular dynamics to hydrodynamics: A novel Galilean invariant thermostat. *J. Chem. Phys.*, 122:114112, 2005.
- [56] D. Talay and L. Tubaro. Expansion of the global error for numerical schemes solving stochastic differential equations. *Stoch. Anal. Appl.*, 8(4):483–509, 1990.
- [57] F. Thalmann and J. Farago. Trotter derivation of algorithms for Brownian and dissipative particle dynamics. *J. Chem. Phys.*, 127:124109, 2007.
- [58] K. P. Travis and C. Braga. Configurational temperature control for atomic and molecular systems. *J. Chem. Phys.*, 128:014111, 2008.
- [59] I. Vattulainen, M. Karttunen, G. Besold, and J. M. Polson. Integration schemes for dissipative particle dynamics simulations: From softly interacting systems towards hybrid models. *J. Chem. Phys.*, 116:3967, 2002.
- [60] L. Verlet. Computer “experiments” on classical fluids. I. Thermodynamical properties of Lennard-Jones molecules. *Phys. Rev.*, 159(1):98, 1967.
- [61] S. Yaghoubi, E. Shirani, A. R. Pishevar, and Y. Afshar. New modified weight function for the dissipative force in the DPD method to increase the Schmidt number. *Europhys. Lett.*, 110(2):24002, 2015.